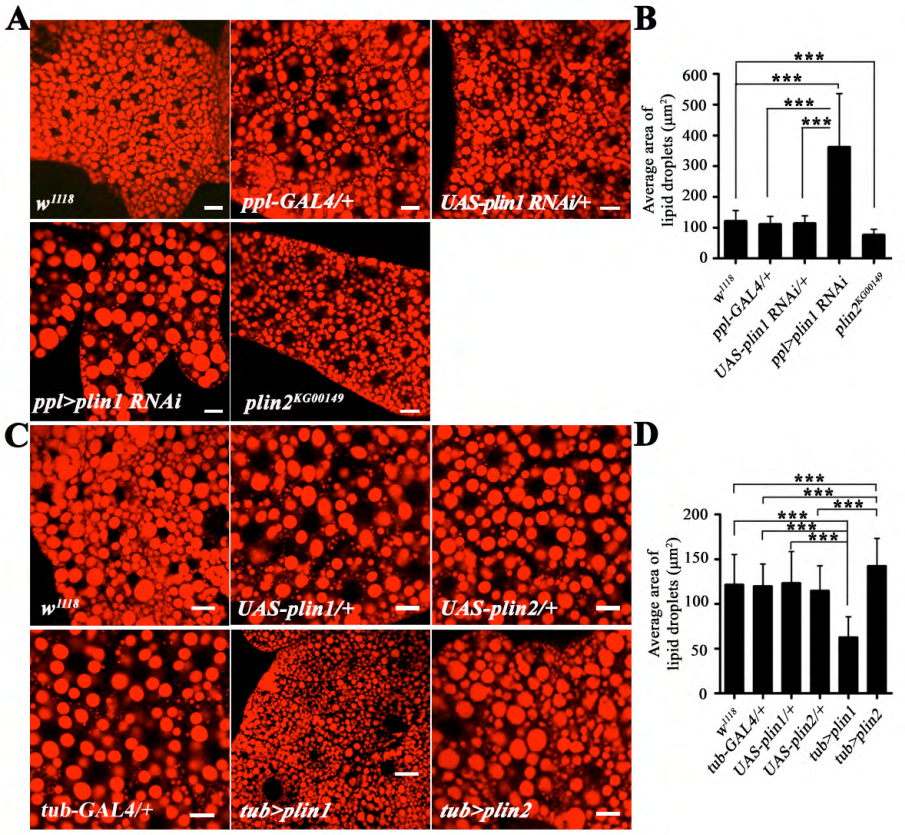

Fig. S1. PLIN1 and PLIN2 have opposite functions. (A) Nile red staining (red) of wandering stage third instar larval fat bodies. *ppl>plin1* RNAi results in large lipid droplets, while *plin2* mutants have small lipid droplets. *ppl>plin1* RNAi is short for *ppl-Gal4>UAS-plin1* RNAi, where *plin1* RNAi is expressed using the *ppl-Gal4* driver. Scale bars: 20μm. (B) Quantification of the size of lipid droplets (LD) shown in (A). The area of the three largest lipid droplets per cell was measured in 50 cells. The average size of the lipid droplets (LD) was calculated. ***p<0.001. (C) Nile red staining (red) of wandering stage third instar larval fat bodies. Overexpression of *plin1* and *plin2* with *tub-Gal4* leads to opposite phenotypes. Scale bars: 20μm. (D) Quantification of the size of lipid droplets shown in (C). ***p<0.001.

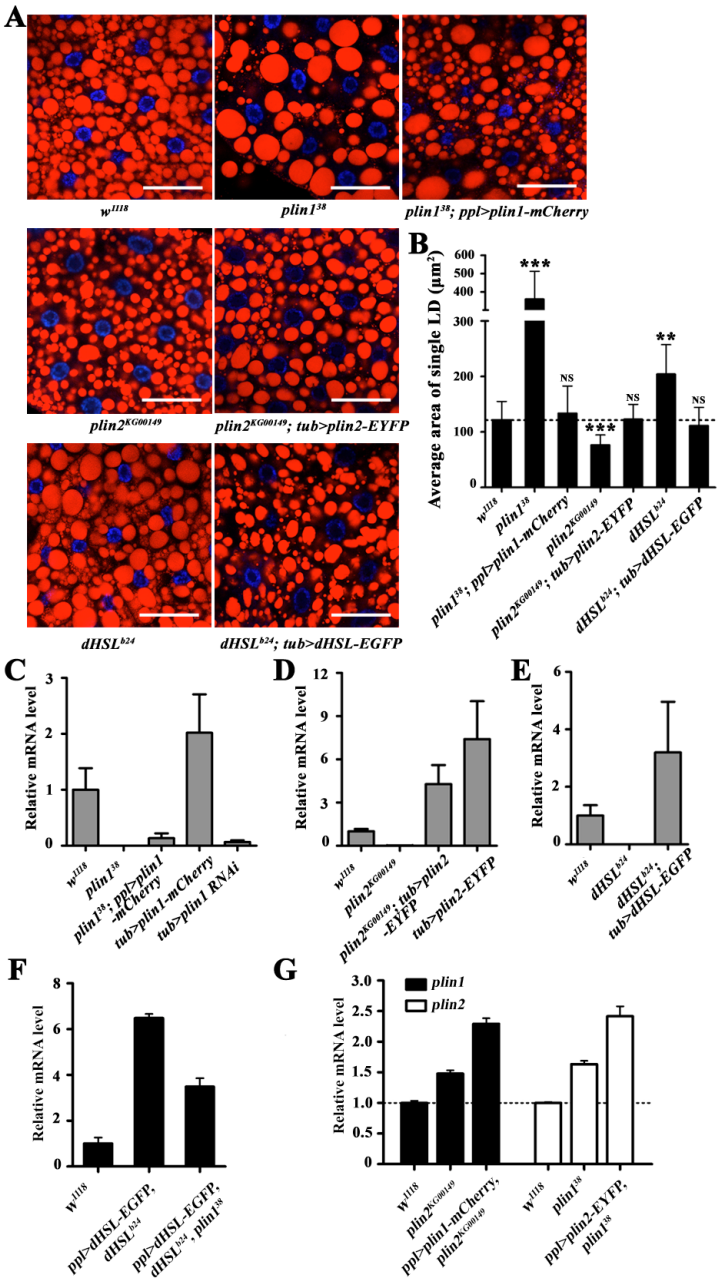

Fig. S2. The fluorescent protein-tagged PLIN1, PLIN2, and dHSL are functional. (A) Nile red staining of wandering stage third instar larval fat bodies. Blue: DAPI staining of nuclei, Scale bar: 50μm. (B) Quantification of lipid droplet size in different genetic backgrounds. NS: non-significant; **p<0.01; ***p<0.001. (C) Relative level of *plin1* mRNA in third instar larvae in different genetic backgrounds assayed by quantitative RT-PCR. (D) Relative level of *plin2* mRNA in third instar larvae in different genetic backgrounds assayed by quantitative RT-PCR. (E-F) Relative level of *dHSL* mRNA in third instar larvae in different genetic backgrounds assayed by quantitative RT-PCR. (G) Relative level of *plin1* and *plin2* mRNA in third instar larvae in different genetic backgrounds assayed by quantitative RT-PCR.

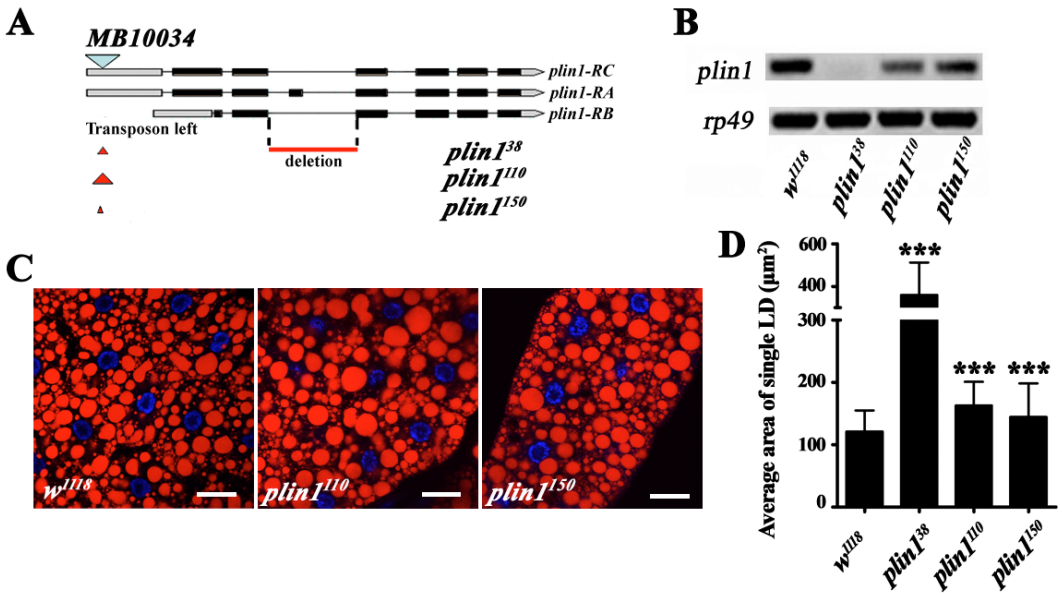

Fig. S3. *plin1* mutants. (A) The genomic structure of the *plin1* locus. Grey box: UTR; black box: coding region. *MB10034* has a *Minos* transposon inserted into the UTR. The *plin1-RA* cDNA was used in this study. Molecular lesions of three *plin1* alleles are shown. The different sized red triangles indicate how much of the transposon element is left in the insertion site. The red line shows the deleted region in $plin1^{38}$. (B) RT-PCR of *plin1* in different genetic backgrounds. Primers are located within the 6th exon of *plin1*. $plin1^{38}$ is likely a null, while $plin1^{110}$ and $plin1^{150}$ are two partial loss-of-function alleles. (C) Nile red staining of wandering stage third instar larval fat bodies. Blue: DAPI staining of nuclei. Scale bar: 20μm. (D) Quantification of lipid droplet size in different genetic backgrounds. ***p<0.001.

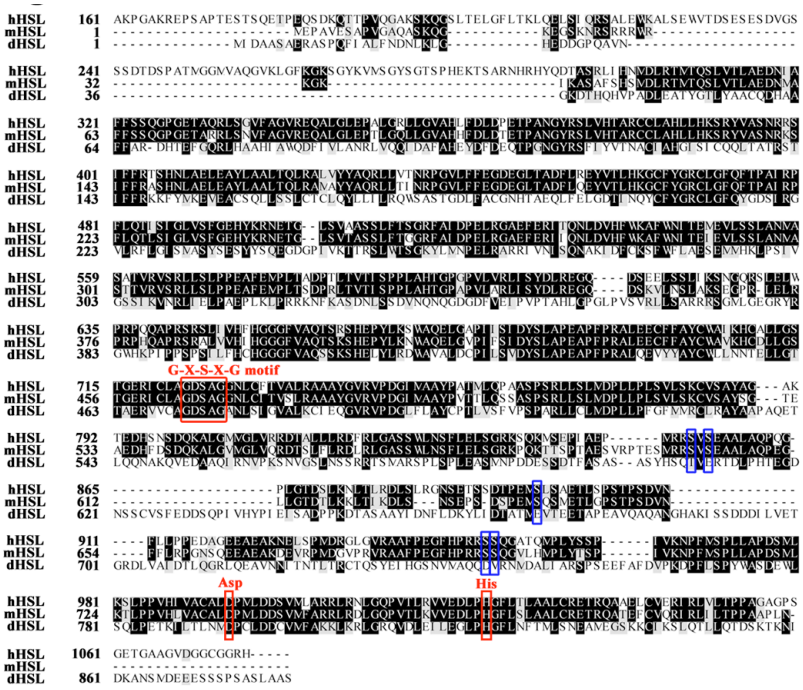

Fig. S4. Protein sequence alignment of HSL in human, mouse, and fly. Sequence alignment of HSL homologous proteins from fly (CG11055), mouse (NP034849) and human (NP725941). The conserved catalytic active site triad (Ser-473 in the G-X-S-X-G motif, Asp-794 and His-824) is marked by red boxes. The five Serine phosphorylation sites found in mouse and human HSL are indicated by blue boxes and are not conserved in dHSL.

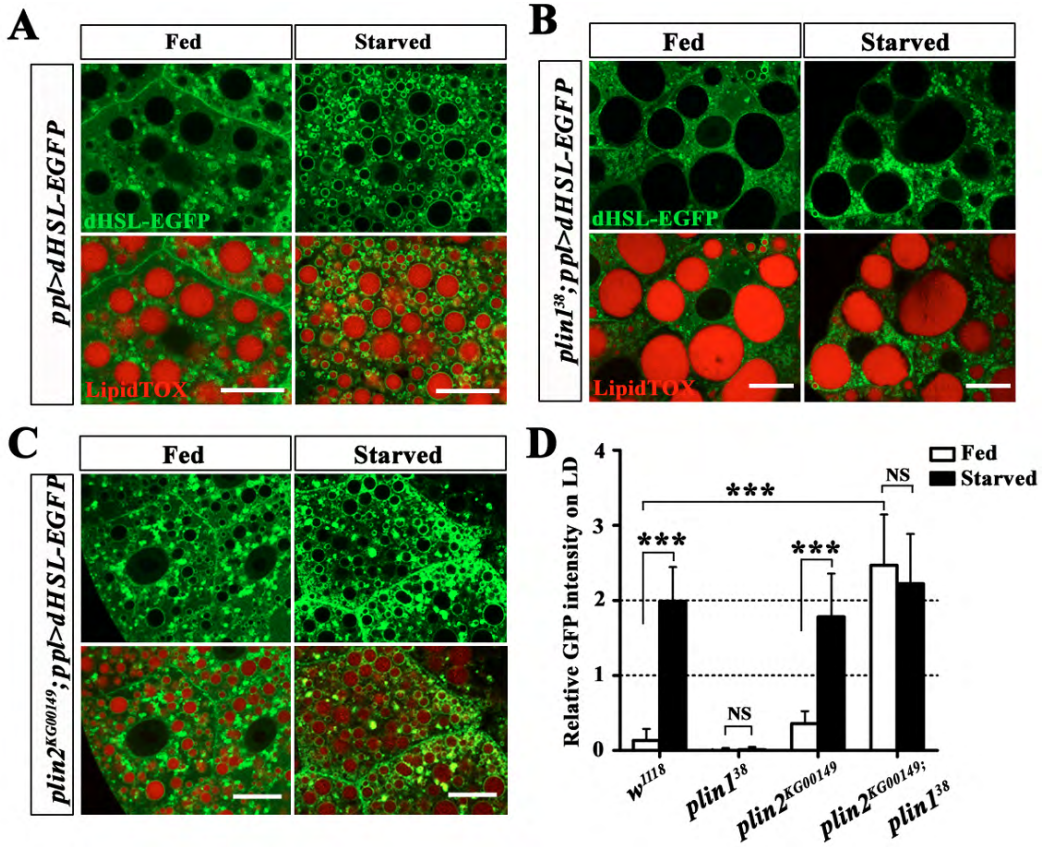

Fig. S5. *plin1* is important for dHSL-EGFP location to lipid droplets. (A-C) Localization of dHSL-EGFP in wild type, *plin1*^{38} and *plin2*^{KG00149} mutant third instar larval fat bodies under both fed and starved conditions. Scale bar: 20μm. (D) Quantification of the lipid droplet localization of dHSL-EGFP in (A-C). dHSL-EGFP localizes to lipid droplets under starved condition in wild type and *plin2*^{KG00149} mutants, but not in *plin1*^{38}mutants. Under fed conditions, dHSL-EGFP is found on some lipid droplets in *plin2*^{KG00149} mutants. NS: non-significant; ***p<0.001.

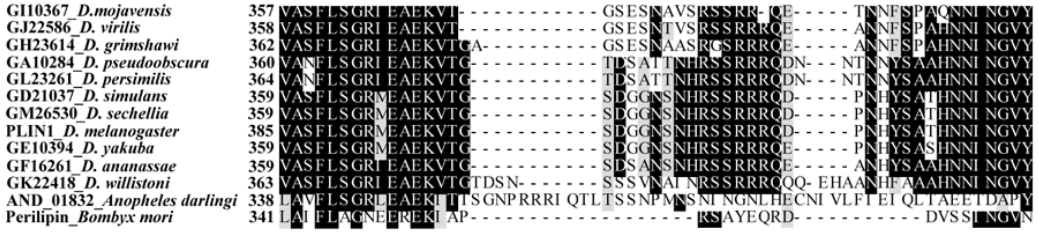

Fig. S6. Sequence alignment of the C-terminal region of PLIN1 in insects. Sequence alignment of the C-terminal region of PLIN1 proteins from *Anopheles darlingi* (EFR29315), *Bombyx mori* (NP001040143), and different species of *Drosophila*.